DISTRIBUTION STATEMENT A. Approved for public release; distribution is unlimited.

Multi-scale Predictability with a New Coupled Non-hydrostatic Global Model over the Arctic Annual Report

Steven Cavallo
University of Oklahoma
School of Meteorology
120 David L. Boren Blvd. Suite 5900
Norman, OK 73072-7307
phone: (405) 325-2439 fax: (405) 325-7689 email: cavallo@ou.edu

William Skamarock
National Center for Atmospheric Research (NCAR)
NCAR Earth System Laboratory, Mesoscale and Microscale Meteorology Division
P.O. Box 3000 Boulder, CO, 80307-3000
phone: (303) 497-8161 fax: (303) 497-8171 email: skamaroc@ucar.edu

Award Number: N00014-121-0328

LONG-TERM GOALS

We are addressing scientific issues related to Arctic weather, sea ice, and the Arctic Oscillation. Our study utilizes a new global, nonhydrostatic atmospheric model called the Model for the Prediction Across Scales (MPAS) to examine a multi-scale feature that is common to the Arctic called tropopause polar vortices (TPVs). The long-term goal is to gain knowledge of the role that TPVs have in longer-term weather and climate prediction. Lifetimes of TPVs can be weeks to months due to their relative position poleward of the polar jet stream and because of the limited heat and moisture in their environments. These factors allow longwave radiative processes to dominate TPV intensity (Cavallo and Hakim 2009; Cavallo and Hakim 2010; Cavallo and Hakim 2012; Cavallo and Hakim 2013). Although longwave radiative cooling rates are on the order of 1-2 K day^{-1}, such cooling rates within a TPV have a significant impact on net intensity on time scales greater than 5-7 days. Temperature anomalies in excess of 10 K imply that thermal gradients are significantly enhanced when TPVs interact with jet streams. Thus we are working under the hypothesis that TPVs are an important and active feature in atmospheric wave breaking, which is a prediction barrier in current numerical weather prediction (NWP) models.

OBJECTIVES

Our primary objective in this project is to evaluate whether the capabilities of MPAS are beneficial for longer-term prediction of multi-scale features such as TPVs and atmospheric wave breaking. The centroidal Voronoi mesh in MPAS allows for local refinement, and the variable-resolution horizontal mesh takes advantage of the unstructured-mesh capabilities of the MPAS nonhydrostatic solver. The variable-resolution meshes are generated such that there is a gradual change in mesh density from the

coarse to the high resolution regions, and as such allow for much more flexible mesh refinement capabilities than approaches using a remapping of a structured mesh. The smooth mesh transitions we use in MPAS stand in contrast to the abrupt mesh transitions used in traditional 2-way nested models such as WRF or in mesh refinement achieved directly through cell division using rectangles or triangles. We are evaluating whether this smooth mesh transition ameliorates many of the difficulties associated with traditional nesting approaches.

APPROACH

Our effort focuses on identifying mechanisms that enhance predictability of physical and dynamical processes in polar regions, which are relatively weak in comparison to lower latitudes (Jung and Co-authors, 2013). Sea ice and TPVs are unique factors of significance in the north polar region, most critical to our understanding and likely to be co-dependent. The importance of synoptic-scale cyclones to the Earth's climate system is well-established, particularly for their role in transporting heat, momentum and moisture from lower-latitudes to the extratropics (e.g., Trenberth and Stepaniak 2003; Eckhardt et al. 2004; Schneider et al. 2006; Boutle et al. 2011). Tropopause dynamics is important for the development of surface cyclones (e.g., Eliassen and Kleinschmidt 1957). TPVs are critical to improving predictability because they are always associated with an upper-level PV anomaly, which is a necessary feature for type B surface cyclogenesis (e.g., Petterssen and Smebye 1971). Surface cyclones can accelerate sea ice loss, as observed in the summer of 2012 when an exceptionally strong cyclone developed over the Arctic Ocean (e.g., Simmonds and Rudeva 2012; Parkinson and Comiso 2013; Kriegsmann and Brümmer 2013; Zhang et al. 2013).

We are working to implement a coupled MPAS-CESM modeling system to determine its ability to capture atmosphere, ocean, and sea-ice feedbacks that may be necessary for accurate prediction on the order of weeks to months. Specific experiments have been designed to examine the evolution, dynamics and predictability of Arctic surface pressure anomalies that are likely associated with the dynamics of tropopause polar vortices (TPVs). During the warm season, Arctic surface pressure anomalies correlate with the phase of the Arctic oscillation (AO) and the flow anomalies have a significant impact on sea ice movement and extent. A correct representation of the ocean and of sea ice is therefore crucial during the warm season since energy fluxes between the atmosphere and ocean depend strongly on the fractional coverage of sea ice. During the cold season, stronger equator-to-pole temperature gradients enhance the strength and influence of the jet stream in polar regions. Thus, atmospheric wave breaking is more frequent, and accounting for global atmospheric interactions between polar regions, midlatitudes, and tropical regions is crucial. Furthermore, more open water increases the potential for the vertical transfer of heat and moisture from the ocean into atmosphere to change atmospheric circulation patterns, particularly during the autumn and early winter months (e.g., Budikova 2009; Deser et al. 2010; Jaiser et al. 2012; Francis and Vavrus 2012; Screen et al. 2013; Vavrus 2013).

Our study approaches this problem by systematically increasing model complexities through a hierarchy of couplings. The first phase began with MPAS atmosphere-only (MPAS-A) experiments, and we are currently transitioning to a second phase that culminates in fully coupled long-term numerical simulations with MPAS-CESM. We have chosen to evaluate the Arctic environment during the summer of 2006 and 2007, which is characterized by two strongly contrasting cyclonic and anticyclonic pressure and tropospheric circulation anomalies. Furthermore, we believe a long-lived TPV and an associated surface cyclone are important factors in the resulting large-scale atmospheric circulation

pattern in the summer of 2006. These cases allow us to answer specific questions regarding the ability of MPAS to reproduce the appropriate AO signatures as well as the ability to predict the evolution of weather patterns that may be important for subsequent sea ice evolution. In particular, we are examining the dynamics of a long-lived TPV and associated surface cyclone where model predictive capability may depend on accurately representing the two-way interactions between atmospheric wind and dynamic sea ice.

WORK COMPLETED

We have expanded our evaluations of MPAS-A sensitivities to physical parameterizations and mesh configuration from the summer warm season to the cold season. The cold season is characterized by a relatively strong polar jet stream, shorter TPV lifetimes, greater arctic to lower-latitude interactions, and high wave activity. Thus we expect this to be a more challenging environment for extended prediction. Our method is to identify particular physical mechanisms and the parameterizations and/or model configuration that accurately represent the long-lived TPV in the summer 2006, then use these expectations to extend our evaluation to other cases so that we can better generalize and develop statistical robustness to the results.

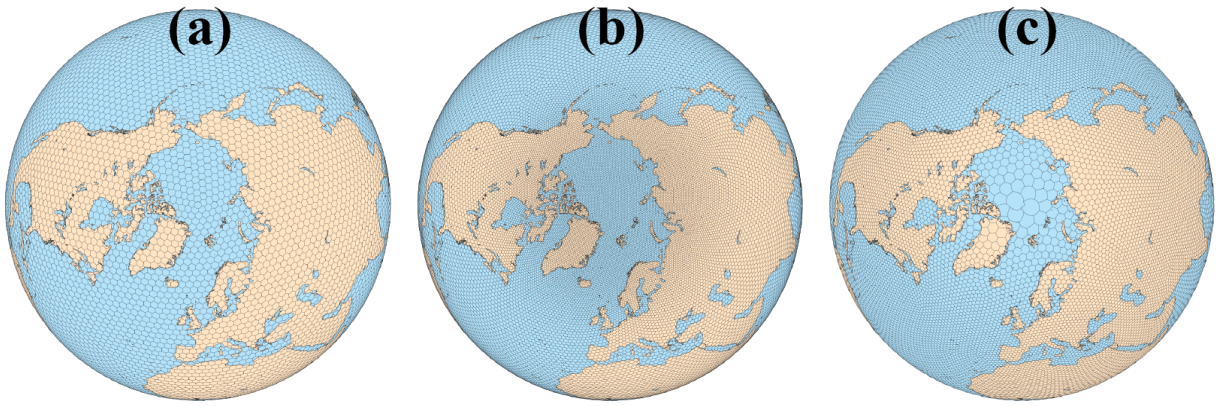

Figure 1: *Schematic of the MPAS C-grid horizontal discretizations that have been implemented for the current study. Comparisons are performed with a (a) uniform mesh containing nearly equal cell spacing of ∼30-km globally, (b) and arctic-refined variable resolution mesh where cell spacing varies from ∼30-km over the Arctic Ocean to ∼60-km in lower latitudes, and (c) a midlatitude-refined variable resolution mesh where cell spacing varies from ∼30-km over midlatitude regions and ∼60-km over the Arctic region.*

The MPAS-A mesh configurations developed for this study are depicted in Fig. 1. We have chosen three different configurations in order to isolate the predictive benefits of having a smooth transition in horizontal resolution, and to further isolate the significance of remote forcings (such as upstream convection) on the prediction of Arctic cyclones. The three meshes are (1) uniform, (2) arctic-refined, and (3) midlatitude-refined, which we will refer to below in a summary of our results.

Additionally, we have spent a significant effort this year on setting up our fully coupled MPAS-CESM configuration. This setup is nearly complete, and we plan to focus future evaluations to experiments using this fully-coupled configuration.

RESULTS

Experiments of the 2006 summer TPV indicate that although there is a sensitivity to physical parameterizations (particularly in the choice of convective parameterization), that our largest errors arise from the specific configuration of the global mesh grid refinement. In the following example, we ask the question: Is the prediction of TPV track and intensity more sensitive to resolving local features of the TPV or remote features upstream of the TPV that impact the environment for which the TPV exists? We hypothesized that midlatitude convection could initiate Rossby waves, and therefore influence the track of the TPV due to changes in the larger-scale atmospheric flow pattern. If Rossby waves influenced the TPV, then the TPV would not be able to strengthen as much as it would if it were in isolation where diabatic processes would dominate its growth mechanisms.

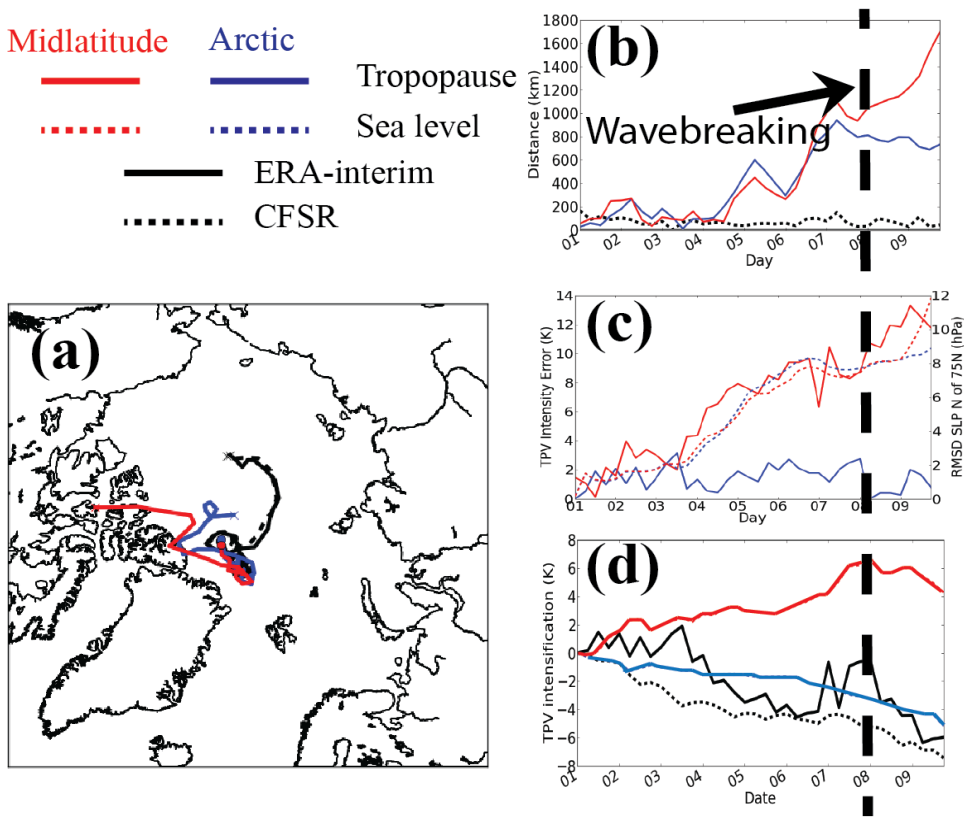

Figure 2: *Tropopause polar vortex (TPV) evolution for MPAS forecasts initialized 01 August 2006 with (a) vortex tracks, (b) track error, (c) intensity and Arctic sea level pressure root mean square difference, and (d) vortex intensification where the initial value of tropopause potential temperature in the vortex core is subtracted from all subsequent values so that negative (positive) values imply the vortex is strengthening (weakening). The color scheme is: (red) Variable resolution midlatitude-refined mesh where cellspacing ranges from 30-km in the midlatitudes to 60-km over the Arctic Ocean, (blue) variable resolution arctic-refined mesh where average cell spacing ranges from 30-km over Arctic to 60-km over middle latitudes, (black) atmospheric reanalyses with ERA-interim (solid) and CFSR (dashed). Solid (dashed) red and blue lines are tropopause potential temperature (sea level pressure) with units of Kelvin (hPa). The vertical dashed line in (b)-(d) denotes the beginning of a tropospheric wavebreaking event of the polar jet stream.*

Results indicate that it is essential to fully resolve the TPV in order to correctly simulate its diabatic processes, and it is less important to resolve remote features that can influence the background circulation in polar regions (Fig. 2). The best prediction of TPV track and intensity is on an arctic-refined mesh, where cell spacing is as low as ∼20-km over the central Arctic Ocean and gradually transitions to ∼60-km at 45°N latitude. In simulations beginning 1 August 2006, the TPV of interest remains over the Arctic as in the ERA-interim and CFSR observation-based reanalyses on the arctic-refined mesh, however on the midlatitude-refined mesh, the TPV erroneously moves out of the Arctic and into northern Canada (Fig. 2a). TPV track differences on the arctic-refined and midlatitude-refined meshes begin to diverge around forecast day 7 (Fig. 2b). Intensity differences are immediately apparent; intensity error in the midlatitude mesh increases at a nearly steady rate while intensity error remains below 2 K through day 9 on the arctic-refined mesh (Fig. 2c). After 1 week, TPV intensity is around 10 K weaker in the midlatitude-refined mesh (Fig. 2d).

We now summarize the reasons as to why finer resolution over the arctic leads to extended predictive skill. During this time period, convection in lower latitudes initiates a Rossby wave which reaches the Arctic around forecast day 7. On the midlatitude-refined mesh, this Rossby wave does not have as strong of an interaction with the weaker TPV. Ultimately, the Rossby wave breaks over the central Arctic Ocean as illustrated in Fig. 3a on forecast day 8 while it breaks south of Svalbard on the midlatitude-refined mesh (Fig. 3b). Subsequently, the circulation from the new anticyclone and the circulation from the cyclonic TPV interact such that the cyclonic TPV remains over the central Arctic Ocean on the arctic-refined mesh, similar to the analyzed evolution from ERA-interim and CFSR. However, because the weaker anticyclone is quickly advected downstream on the midlatitude-refined mesh, the TPV track on this mesh diverges from that analyzed in ERA-interim and CFSR, and diverges from the solution on the arctic-refined mesh (Recall Fig. 2b). Once the wave breaking event has completed, there is an irreversible impact on both the atmospheric circulation over the Arctic Ocean and on the polar jet stream (Fig. 3c).

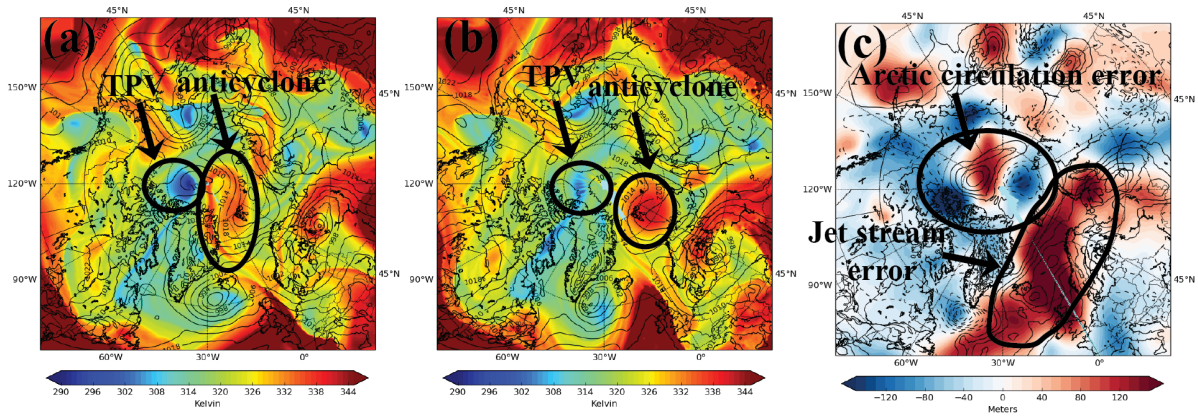

Figure 3: *(a)-(b) MPAS forecasts of tropopause potential temperature (colors; units = Kelvin) and sea level pressure (contours; units = hPa) on 08 August 2006 at 00 UTC on the (a) Arctic refined mesh and (b) midlatitude refined mesh. (c) Difference in atmospheric circulation between the Arctic and midlatitude refined meshes on 09 August 2006 at 12 UTC as shown through 500 hPa geopotential heights (colors) and sea level pressure (contours; solid are positive differences, dashed are negative differences). Forecasts are initialized 01 August 2006 at 00 UTC. See Figure 1 for description of arctic- and midlatitude-refined meshes.*

We believe the simulated differences between the TPV feedback with the Rossby wave ultimately had a substantial impact on the longer-term atmospheric circulation patterns. A stronger TPV is more likely to come into phase with low-level baroclinicity to generate and strengthen a surface cyclone. A stronger surface cyclone will be associated with a stronger warm conveyor belt, transporting moisture deeper into the Arctic along it. Stronger magnitudes of latent heating along the warm conveyor belt will further strengthen the developing upper-level anticyclonic ridge above and downstream of the level of maximum latent heating while the circulation of the TPV will advect this air further poleward. Ultimately, the TPV acts to amplify the wave pattern on the tropopause so that these waves are more likely to break more quickly than if the TPV did not have an influence. We will investigate this hypothesis in the remainder of the study: Since Rossby wave breaking is a barrier to extended prediction, TPVs are an important mechanism that can influence the character of wave breaking and hence longer-term prediction. Thus, in order to improve the prediction of sea ice, it may be important to focus on the dynamics of Rossby wave breaking with the consideration of TPVs.

Given that the intensity of TPVs may be important to predict in order to more accurately predict Rossby wave breaking, we now examine the physical mechanisms occurring within the TPV leading up to the differences. Intensity forecasts between the arctic- and midlatitude-refined meshes diverge immediately in the MPAS-A forecasts initialized 1 August 2006. We quantify vortex intensity using Ertel potential vorticity (EPV):

$$\Pi = \frac{\vec{\omega}_a}{\rho} \cdot \nabla\theta \tag{1}$$

where $\vec{\omega}_a$ is the three-dimensional absolute vorticity vector, ρ is the density of air, θ is potential temperature, and $\nabla = \left(\frac{\partial}{\partial x}, \frac{\partial}{\partial y}, \frac{\partial}{\partial z}\right)$ is the gradient operator. We evaluate changes in vortex intensity through the EPV tendency (e.g., Pedlosky, 1992):

$$\frac{D\Pi}{Dt} \simeq \frac{\vec{\omega}_a}{\rho} \cdot \nabla \left(\underbrace{\dot{\theta}_{longwave}}_{\text{A}} + \underbrace{\dot{\theta}_{latent\,heating}}_{\text{B}} + \dot{\theta}_{other} \right) \tag{2}$$

where $\dot{\theta}_{longwave}$ is the longwave radiative potential temperature tendency, $\dot{\theta}_{latent\,heating}$ is the potential temperature tendency due to latent heating, and $\dot{\theta}_{other}$ is the potential temperature tendency from all other diabatic tendencies, including those from shortwave radiative heating, convection, planetary boundary layer effects, and tendencies resulting from explicit mixing processes. The thermodynamic tendency terms are obtained directly after their computations in the model parameterizations.

To illustrate the difference in physical mechanisms leading to differences in intensity, we present vertical averages and cross sections comparing diabatic forcings between the arctic- and midlatitude-refined meshes near the TPV core in the MPAS forecast at a snapshot in time on 2 August 2006 at 00 UTC. The generation of EPV from longwave radiative mechanisms (Term A in equation (2)) has previously been shown to be the primary contribution to TPV intensification over longer time scales (e.g., Cavallo and Hakim, 2013). In this example, the positive vertical gradient (encircled with the label '1' in Fig. 4a) extends through a broad depth of the atmospheric column inside the TPV around the tropopause level on the arctic-refined mesh, implying vortex intensification from (2). However, this region of positive EPV generation due to longwave radiation is weaker at the tropopause and more strongly impacted by clouds in the midlatitude-refined mesh (Fig. 4b). Latent heating tendencies dominate on the midlatitude-refined mesh, contributing to strong destruction of Π that substantially

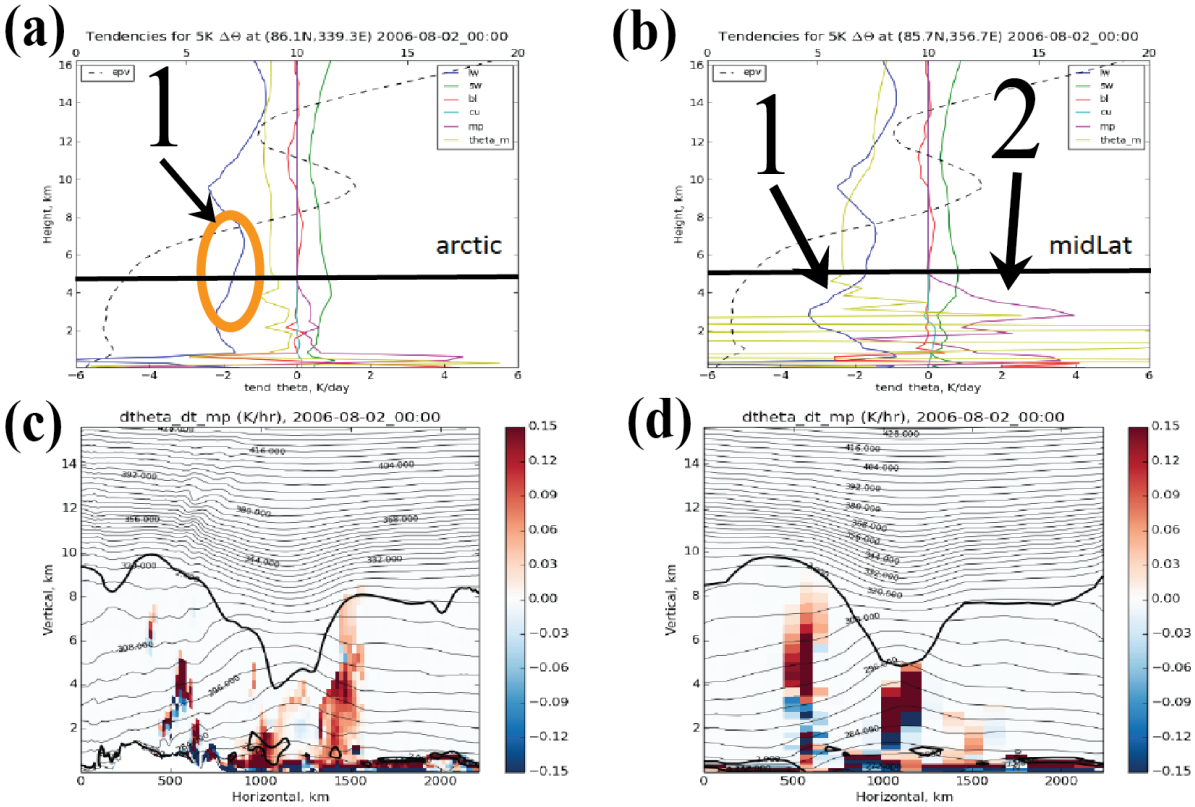

Figure 4: *(a)-(b) Vertical profiles and (c)-(d) height–location cross sections of diabatic θ tendencies from 24-h MPAS forecasts on the (a),(c) arctic-refined mesh and (b),(d) midlatitude-refined mesh on 2 August 2006 at 00 UTC. Units are K day^{-1} in (a)-(b) and K hr^{-1} in (c)-(d). Vertical profiles in (a)-(b) are averaged within a spatial area defined by all locations within a 5 K contour surrounding the vortex core minimum tropopause potential temperature. The numbers '1' and '2' in (a) and (b) are referred to in the text. The solid, black horizontal line denotes the level of the tropopause.*

weaken the vortex (as implied by the negative vertical gradient in Term B in equation (2) in the upper-troposphere encircled with the label '2' in Fig. 4b). On the arctic-refined mesh, cloud patterns (inferred from latent heating tendencies) are more resolved into two separate bands, one shallow layer under the vortex core and one deep layer to the east of the vortex core (Fig. 4c). On the midlatitude-refined mesh, there is a single, deep cloud layer directly underneath the vortex core (Fig. 4d). This lends evidence to the capability of microphysical parameterizations to accurately represent important banded structures of latent heating (closer to what is observed) given adequate grid spacing.

Since we have identified important barriers to predictability in the 2006 summer case with MPAS, we have begun to examine other cases, which occur during the cold season when prediction is more difficult. In contrast to the summer warm season, the cold season is characterized by a relatively strong polar jet stream, shorter TPV lifetimes, greater arctic to lower-latitude interactions, and high wave activity. Surface forcings in the cold-seasons of the Arctic are directed from the surface to the atmosphere due to the lack of shortwave radiative heating (Serreze et al. 2007). Furthermore, the stronger polar jet stream and more active waveguide increases the potential for the formation of extreme

jet streams due to the enhanced thermal gradient along the tropopause associated with both the jet stream and from the ∼20 K average thermal anomaly of the TPV itself. Stratospheric processes likely have significance during the cold season given that sudden stratospheric warmings are nearly always preceded by tropospheric blocking events (Martius et al. 2009), and the onset of tropospheric blocking usually occurs in association with breaking Rossby waves near the tropopause (e.g. Pelly and Hoskins 2003; Woolings et al. 2008). Given the role that TPVs have in Rossby wave breaking, the cases we examine with TPVs are expected to strengthen knowledge regarding regime changes associated with the AO.

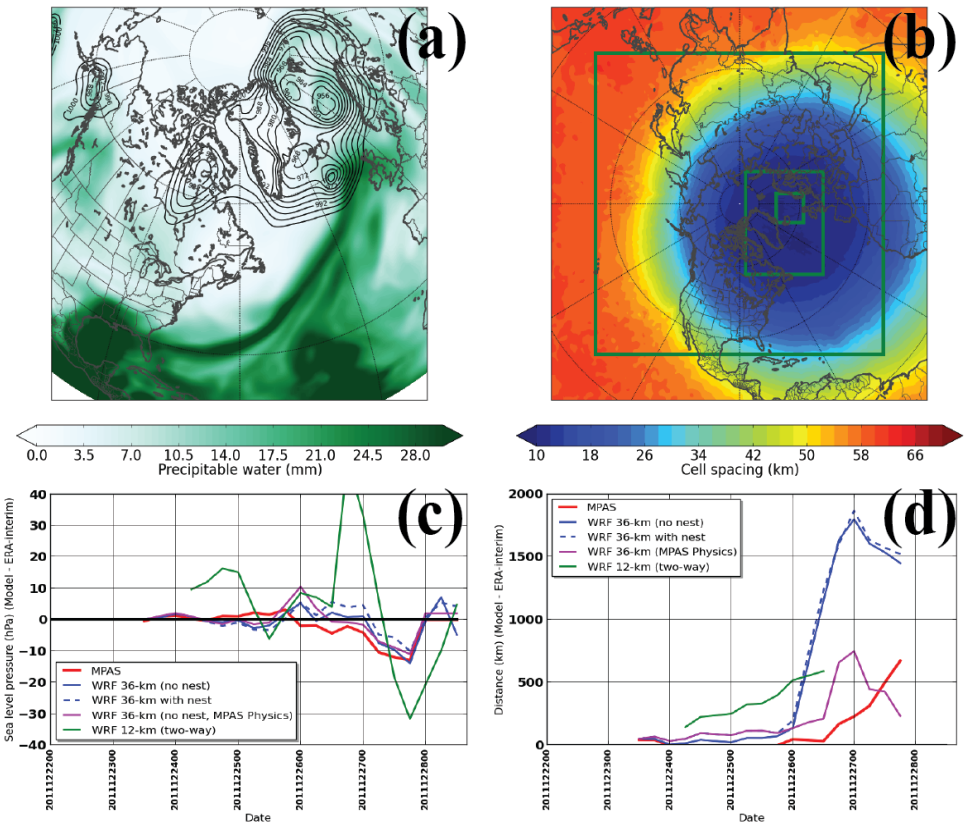

Figure 5: *Example of a high impact arctic-to-tropical interaction event on 25 December 2011 (named Cyclone Dagmar by the Norwegian Weather Service and Cyclone Patrick in Germany). Shown is an evaluation of MPAS forecasts containing a variable resolution mesh with Weather Research and Forecasting (WRF) model nested domains. ERA-interim analysis of precipitable water (colors; mm) and sea level pressure (contours; hPa). Experimental configuration with (b) Cell spacing of MPAS (colors), with a refined mesh centered over Iceland compared with WRF nested domains in green. Comparison of MPAS-A and WRF nests for 5-d forecasts of Cyclone Dagmar's (c) sea level pressure (hPa) and (d) track difference with respect to ERA-interim reanalysis (km).*

The first case we have examined is in collaboration with DRI PI Dr. Melvyn Shapiro for the case of Cyclone Dagmar, which occurred 25-26 December 2011. Cyclone Dagmar was a high-impact extreme surface cyclone in Europe, and demonstrates many benefits of higher resolution, global, nonhydrostatic numerical modeling with MPAS. This event was characterized by an extreme jet stream associated with a TPV, subsequent Rossby wave breaking, and strong moisture transport from tropical regions into the

Arctic (Fig. 5a). However, Dagmar's 964 hPa central minimum sea level pressure was spatially small in scale, developing rapidly over the North Atlantic Ocean. We performed forecasts on an MPAS variable resolution domain with ∼15-km cell spacing centered over Iceland to ∼60-km cell spacing outside the area of mesh refinement (Fig. 5b). The MPAS forecasts were compared to a WRF nested configuration using 36-km grid spacing in the outer domain, one nest with 12-km grid spacing over the region Dagmar intensified most rapidly, and an inner 4-km nest upstream of Dagmar's landfall in Norway. Both WRF and MPAS predicted a strong cyclone, however, due to the fast movement of Dagmar, global variable resolution MPAS-A forecasts outperformed nested WRF-ARW forecasts in track (Fig. 5c,d). Forecasts on the higher-resolution WRF nests resulted in the greatest track errors, with greater bias than lower resolution larger-domain WRF forecasts. We are currently examining the hypothesize that since there was a strong connection with tropical moisture, and there was an extreme jet and TPV in the vicinity, that diabatic forcings had a significant impact. We will continue to generalize our findings by taking an in-depth examination of this case with Dr. Shapiro, and extend the knowledge gained to other cases during the remainder of this project.

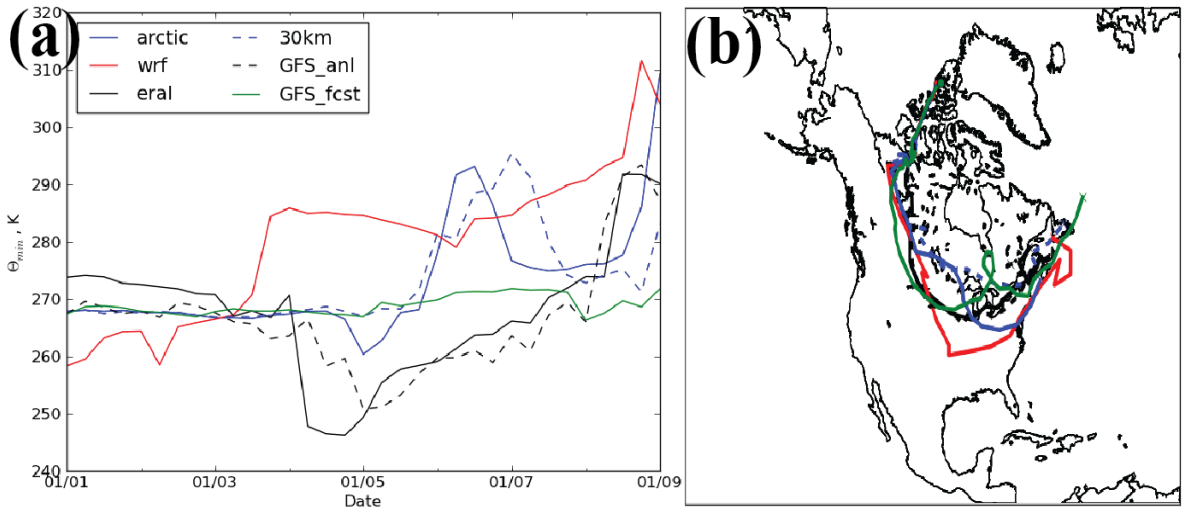

Figure 6: *Comparison of forecasts for the January 2014 "polar vortex." (a) TPV intensity (Kelvin) and (b) vortex tracks for the MPAS-A arctic-refined mesh (solid blue), MPAS-A uniform resolution 30-km mesh (blue dashed), a WRF Northern Hemisphere-wide domain with 30-km grid spacing (red), GFS forecasts (green), ERA-interim reanalyses (black), and GFS final analyses (dashed black). All forecasts are initialized on 1 January 2014 at 00 UTC.*

We will continue to increase the number of cases we examine in order to better generalize our results. In order to readily compare our MPAS test cases with WRF forecasts, we are automatically generating WRF forecasts on the outer WRF domain shown in Fig. 5b. Our WRF forecasts are performed daily at 00 UTC at http://arctic.som.ou.edu/realtime.php. One case we have begun to examine during this past year from this configuration is the so-called "polar vortex" case of January 2014. This case was characterized by a strong TPV that moved well into the middle latitudes over the United States to result in an unusually persistent period of cold temperatures over North America. Despite this event occurring on the region of mesh refinement in the MPAS arctic-refined mesh, MPAS forecasts on the arctic-refined grid generally outperformed the WRF forecasts in intensity, and particularly in TPV track (Fig. 6). Both this case, and the case of cyclone Dagmar highlight the weakness of regional model

dependence on lateral boundary conditions for cold-season events where tropical-to-arctic interactions span a large geographic range.

IMPACT/APPLICATIONS

The MPAS modeling system will potentially be a useful tool for longer-term prediction needs. Such applications are those pertaining to regional climate predictions or those where global and/or coupled interactions can have significant impacts on forecast skill. Examples of such processes include the Madden-Julien Oscillation, the El Nino Southern Oscillation, the Arctic Oscillation, and sea ice variability, where longer-term prediction is required beyond the range of significant forecast skill capability exhibited by traditional NWP models. Furthermore, it is not clear whether traditional Global Climate Models (GCMs) have the capability of accurate prediction of finer-scale processes, which may be crucial for predicting initial perturbations that grow upscale in time and space.

TRANSITIONS

None.

RELATED PROJECTS

None.

REFERENCES

I. A. Boutle, S. E. Belcher, and R. S. Plant. Moisture transport in midlatitude cyclones. 137(655): 360–373, 2011.

D. Budikova. Role of Arctic sea ice in global atmospheric circulation. *Glob. Planet. Change*, 68: 149–163, 2009. doi: 10.1016/j.gloplacha.2009.04.001.

S. M. Cavallo and G. J. Hakim. Potential vorticity diagnosis of a tropopause polar cyclone. 137(4): 1358–1371, 2009.

S. M. Cavallo and G. J. Hakim. The composite structure of tropopause polar cyclones from a mesoscale model. 138(10):3840–3857, 2010. doi: 10.1175/2010MWR3371.1.

S. M. Cavallo and G. J. Hakim. Radiative impact on tropopause polar vortices over the arctic. 140(5): 1683–1702, 2012.

S. M. Cavallo and G. J. Hakim. The physical mechanisms of tropopause polar cyclone intensity change. 70:3359–3373, 2013.

C. Deser, R. Tomas, M. Alexander, and D. Lawrence. The seasonal atmospheric response to projected Arctic sea ice loss in the late 21st century. 23(2):333–351, 2010.

S. Eckhardt, A. Stohl, H. Wernli, P. James, C. Forster, and N. Spichtinger. A 15-year climatology of warm conveyor belts. 17(1):218–237, 2004.

A. Eliassen and E. Kleinschmidt. *Handbuch der Physik*, volume 48. Springer Verlag, 1957.

J. A. Francis and S. J. Vavrus. Evidence linking Arctic amplification to extreme weather in mid-latitudes. 39(L06801), 2012. doi: 10.1029/2012GL051000.

R. Jaiser, K. Dethloff, D. Handorf, A. Rinke, and J. Cohen. Planetary- and baroclinic-scale interactions between atmospheric and sea ice cover changes in the Arctic. *Tellus A*, 64(11595), 2012. doi: 10.3402/tellusa.v64i0.11595.

T. Jung and Co-authors. WWRP Polar Prediction Project science plan. polarprediction.net/fileadmin/user_upload/Home/Documents/WWRP-PPP%20Science%20Plan%20FInal%2019Mar2013.pdf, 2013. Accessed: 2014-01-09.

A. Kriegsmann and B. Brümmer. Cyclone impact on sea ice in the central Arctic Ocean: A statistical study. *The Cryosphere Discussions*, 7:1141–1176, 2013.

O. Martius, L. M. Polvani, and H. C. Davies. Blocking precursors to stratospheric sudden warming events. 36, 2009. doi: 10.1029/2009GL038776.

C. L. Parkinson and J. C. Comiso. On the 2012 record low Arctic sea ice cover: Combined impact of preconditioning and an August storm. 40(4):1356–1361, 2013. doi: 10.1002/grl.50349.

J. Pedlosky. *Geophysical Fluid Dynamics*, volume 84. Springer, second edition, 1992.

J. L. Pelly and B. J. Hoskins. A new perspective on blocking. 60:743–755, 2003.

S. Petterssen and S. J. Smebye. On the development of extratropical cyclones. 97:457–482, 1971.

T. Schneider, K. L. Smith, P. A. OGorman, and C. C. Walker. A climatology of tropospheric zonal-mean water vapor fields and fluxes in isentropic coordinates. 19(22):5918–5933, 2006.

J. A. Screen, I. Simmonds, C. Deser, and R. Tomas. The atmospheric response to three decades of observed Arctic sea ice loss. 26:1230–1248, 2013. doi: 10.1175/JCLI-D-12-00063.1.

M. C. Serreze, A. P. Barrett, A. G. Slater, M. Steele, J. Zhang, and K. E. Trenberth. The large-scale energy budget of the Arctic. 112(D11122), 2007. doi: 10.1029/2006JD008230.

I. Simmonds and I. Rudeva. The great Arctic cyclone of August 2012. 39(L23709), 2012. doi: 10.1029/2012GL054259.

K. E. Trenberth and D. P. Stepaniak. Covariability of components of poleward atmospheric energy transports on seasonal and interannual time-scales. 16:36913705, 2003.

S. J. Vavrus. Extreme arctic cyclones in CMIP5 historical simulations. 40(23):6208–6212, 2013.

T. Woolings, B. Hoskins, M. Blackburn, and P. Berrisford. A new Rossby wave-breaking interpretation of the North Atlantic Oscillation. 65:609–626, 2008. doi: 10.1175/2007JAS2347.1.

J. Zhang, R. Lindsay, A. Schweiger, and M. Steele. The impact of an intense summer cyclone on 2012 Arctic sea ice retreat. 40(4):720–726, 2013. doi: 10.1002/grl.50190.